An Accurate Field Matching Analysis of Waveguides of Complex Cross-Sectional Geometry Loaded with Magnetized Ferrite Rods

Michal Okoniewski, *Member, IEEE,* and Jerry Mazur

Abstract—**Many structures, such as ferrite phase shifters and rectangular waveguides loaded with ferrite or dielectric rods of circular cross-section are difficult to analyze. We have developed a field-matching technique capable of analysis of waveguides of complex cross-sectional geometry comprising longitudinally magnetized ferrite rods. The method has been implemented on a PC computer equipped with a Microwave i860 board. Computations of inner products by FFT resulted in three-fold increase in computational speed and two-fold reduction of computer memory required. The method provides results with high accuracy and within a reasonable computing time. Convergence properties, numerical and experimental results are presented.**

I. Introduction

WAVEGUIDES of complex cross-sections containing dielectric or ferrite materials pose challenging analytical problems. Earlier analyses were reviewed by Saad in 1985 [1]. Recent progress in numerical techniques has resulted in new solution methods applied to complex shape guides (for an extensive list of references see [2]). In [3] an attempt was made to apply time domain techniques to analyze structures comprising ferrite materials. Although time domain techniques have potentials to analyze complicated structures, the implementation used in that paper relied on a complicated equivalent circuit representation of ferrite media, and as a result simulations of only simple homogeneous waveguides were reported.

In this paper we describe an extension (first presented in [4]) of the method based on the mode matching technique and previously reported to analyze planar circuits [5]–[7] and complex, dielectric loaded waveguides [8]. Waveguides having complicated cross-sectional geometry and comprising circularly-cylindrical ferrite-dielectric rods magnetized in a longitudinal direction can be analyzed with this method. Although the field matching is not usually recognized as a very flexible method, the formulation we use let us analyze a wide class of waveguides (see Figs. 2 and 3). This class of waveguides includes rectangular waveguides loaded with ferrite rods, which have not been rigorously analyzed before.

Following the description of the analysis, convergence properties of the method are discussed. Numerical results and experimental data validating our theory are given. The examples of new, potentially useful structures (e.g., ferrite loaded waveguides of crossed-rectangular and finned-circular cross sections) are outlined.

Manuscript received November 10, 1993; revised July 20, 1994.

M. Okoniewski is with the Department of Electrical and Computer Engineering.University of Victoria, Victoria, BC, Canada V8W 3P6.

J. Mazur is with the Technical University of Gdańsk, Telecommunication Institute, 80-952 Gdańsk, Poland.

IEEE Log Number 9408580.

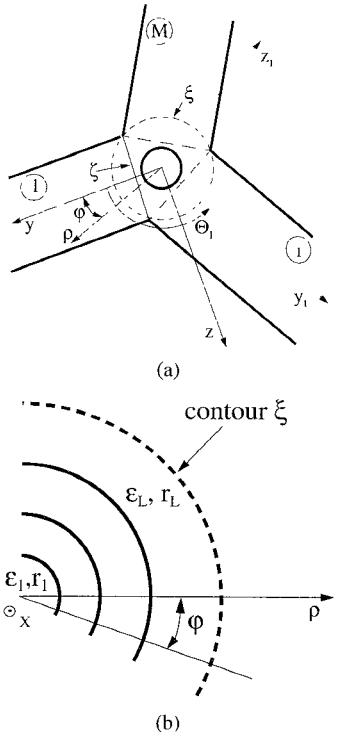

Fig. 1. Analyzed structure. (a) Schematic presentation. (b) Structure of IG.

II. Analysis

A cross-sectional geometry of the analyzed waveguide is shown in Fig. 1(a.) The following assumptions are made:

1) the time dependence is harmonic (the term $\exp(j\omega t)$is suppressed for the sake of clarity);
2) the structure is homogeneous in the x direction (perpendicular to the plane of the drawing) and the x dependence is exponential, $\exp(-j\beta x)$, where β is the propagation constant;
3) all conductors in the structure are perfect and constitutive parameters are linear and time invariant;

Note, however that ferrite and dielectric materials are not assumed lossless.

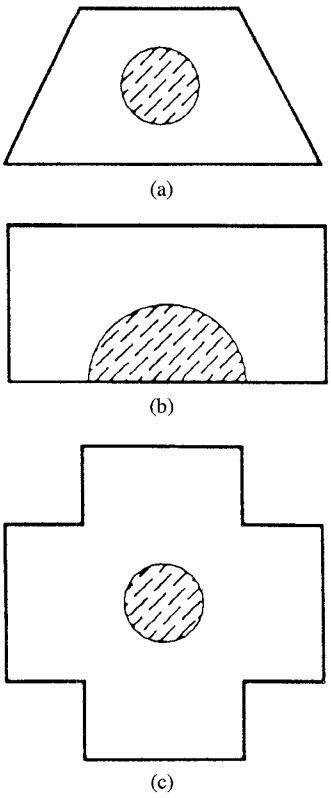

Fig. 2. Examples of ferrite or dielectric loaded structures which can be analyzed by our method. (a) Trapezoidal waveguide. (b) "Mage" guide. (c) Cross-rectangular guide. AG's assumed as rectangular guides. Other examples in Fig. 3.

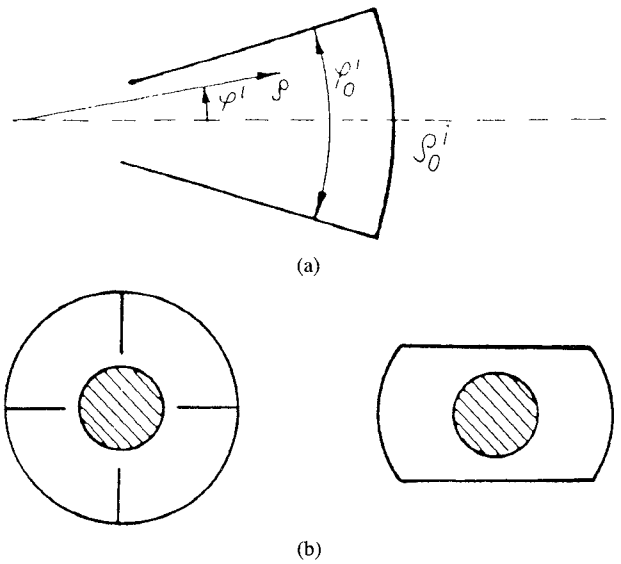

Fig. 3. AG as (a) sectoral guides and (b) examples of waveguides with sectoral AG's.

Essential steps of the analysis are as follows:

1) We divide the structure into regions, in which solutions of Maxwell's equations can be found relatively easily, namely:
   - Inner cylindrical guide (IG) is defined in cylindrical coordinates (delineated with curve ξ—Fig. 1(a)). IG is transversely inhomogeneous and consists of an arbitrary number of cylindrical layers. All layers but the outer most one can be longitudinally magnetized ferrites.
   - Isotropic and homogeneous attached guides (AG). These guides can take a variety of shapes, for instance a rectangular guide open at one side (as in Fig. 1a), or a sectoral guide (Fig. 3).
2) We find the general solution of Maxwell's equations in IG. Here we exploit the *transfer matrix* concept (modified for the case of a ferrite IG) to treat the layered structure of IG [8], and express the field quantities in the outermost layer of IG in terms of the amplitudes of the innermost one.
3) We find the field in AG's in terms of series of eigenfunctions fulfilling all the boundary conditions except those on the interface with IG.
4) Now we match the fields, i.e., match the general solutions found in the regions described. This yields a set of function equations.
5) We transform this set of equations into an algebraic matrix system using the functional analysis techniques and truncating the series. By elimination of the unknown set of amplitudes in IG region we arrive at the homogeneous system of equations. Setting the determinant of the system's matrix to zero, we get the dispersion equation.

A. Fields in IG Region

To find the field vectors in the outermost cylinder of IG we use the transfer matrix concept [9] adopted for cylindrical ferrite media. General solutions to Maxwell's equations in an arbitrary, say lth, cylinder of IG are obtained first. Since this layer is filled with ferrite medium magnetized in the direction of propagation, the electromagnetic field is governed by the following pair of coupled equations [10]:

$$\left(\nabla_t^2 - \beta^2 + k_0^2 \epsilon_l \mu_{\text{eff}_l}\right) D_x + j\beta k_0 \epsilon_l \frac{\mu_{a_l}}{\mu_l} \tilde{H}_x = 0$$
$$\left(\nabla_t^2 - \frac{1}{\mu_l}\beta^2 + k_0^2 \epsilon_l\right) \tilde{H}_x - j\beta k_0 \frac{\mu_{a_l}}{\mu_l} D_x = 0 \qquad (1)$$

where D is an electric flux and $\tilde{H}$ is proportional to magnetic field—$\tilde{H} = \sqrt{\epsilon_0 \mu_0} H$, while μ_{a_l}, μ_l denote the relative off-diagonal and diagonal elements of the permeability tensor, respectively, μ_{eff_l} stands for the relative effective permeability [11], ϵ_l is the relative permittivity, and $k_0 = \omega\sqrt{\epsilon_0 \mu_0}$.

We seek the solution to (1) in terms of series of eigenfunctions

$$D_x^{ol} = \sum_{k=-\infty}^{+\infty} D_{xl}^k e^{-j\beta x} \qquad \tilde{H}_x^{ol} = \sum_{k=-\infty}^{+\infty} \tilde{H}_{xl}^k e^{-j\beta x}. \qquad (2)$$

Each eigenfunction consists of coupled partial waves $\mathcal{D}_x$ and $\mathcal{H}_x$

$$D_{xl}^k = \mathcal{D}_{xl}^k + R_l \mathcal{H}_{xl}^k \qquad \tilde{H}_{xl}^k = S_l \mathcal{D}_{xl}^k + \mathcal{H}_{xl}^k \qquad (3)$$

defined as

$$\mathcal{D}_{xl}^k = \left[A_{1l}^k J_k(\chi_{l_1}\rho) + A_{2l}^k Y_k(\chi_{l_1}\rho)\right] e^{jk\varphi}$$
$$\mathcal{H}_{xl}^k = \left[B_{1l}^k J_k(\chi_{l_2}\rho) + B_{2l}^k Y_k(\chi_{l_2}\rho)\right] e^{jk\varphi} \qquad (4)$$

where k is an integer number, and the eigenvalues $\chi_{l_{1,2}}$ can be found from the following expression:

$$\chi_{l_{1,2}} = \sqrt{\frac{1}{2}\left[(a+c) \mp \sqrt{(a+c)^2 - 4(ac-bd)}\right]} \quad (5)$$

where

$$a = k_0^2 \epsilon_l \mu_{\text{eff}_l} - \beta^2 \qquad b = j\beta k_0 \epsilon_l \frac{\mu_{a_l}}{\mu_l}$$
$$c = k_0^2 \epsilon_l - \frac{1}{\mu_l}\beta^2 \qquad d = j\beta k_0 \frac{\mu_{a_l}}{\mu_l}$$

and $J_k(\cdot)$, $Y_k(\cdot)$ are Bessel and Neumann or modified Bessel and McDonald functions, depending on the sign of $k_d^2 - \beta^2$.

Note that the coupling coefficients R_l and S_l

$$S_l = \frac{\chi_{l_1}^2 - a}{b} \qquad R_l = \frac{\chi_{l_2}^2 - c}{d}$$

vanish when infinite bias magnetization H_i is applied.

Once we have obtained the longitudinal field components, the transverse vectors may be computed from

$$\begin{bmatrix} E_\rho & \tilde{H}_\rho \\ E_\varphi & \tilde{H}_\varphi \end{bmatrix} = \begin{bmatrix} -\frac{\jmath k}{\rho} & \frac{\partial}{\partial \rho} \\ \frac{\partial}{\partial \rho} & \frac{\jmath k}{\rho} \end{bmatrix} \cdot \left(\begin{bmatrix} jk_0/\epsilon_0 S_l & -jk_0 \\ -\frac{j\beta}{\epsilon_0 \epsilon_l} & k_0 \frac{\mu_a}{\mu} - \frac{j\beta S_l}{\mu} \end{bmatrix} \frac{1}{\chi_{l_1}^2} \mathcal{D}_x + \begin{bmatrix} jk_0/\epsilon_0 & -jk_0 R_l \\ -\frac{\jmath\beta}{\epsilon_0 \epsilon_l} R_l & k_0 \frac{\mu_a}{\mu} R_l - \frac{j\beta}{\mu} \end{bmatrix} \frac{1}{\chi_{l_2}^2} \mathcal{H}_x \right). \quad (6)$$

Let us now impose the continuity conditions between two adjacent IG layers. Due to the orthogonality of $\{e^{\jmath k\varphi}\}$ on the layer interfaces, we can consider continuity for each eigenfunction separately. Therefore, for the field components generated by kth eigenfunction, we have

$$E_{\varphi k}^{\circ l} = E_{\varphi k}^{\circ l+1} \qquad E_{xk}^{\circ l} = E_{xk}^{\circ l+1} \quad (7)$$
$$\tilde{H}_{\varphi k}^{\circ l} = \tilde{H}_{\varphi k}^{\circ l+1} \qquad \tilde{H}_{xk}^{\circ l} = \tilde{H}_{xk}^{\circ l+1}. \quad (8)$$

Substituting the formulas in (2), and quantities obtained from (6) for the field components, we can rewrite (7) in a matrix form relating amplitudes of eigenfunctions in lth and $(l+1)$ layers

$$\underline{\underline{X}}_l^k \cdot \underline{A}_l^k = \underline{\underline{X}}_{l+1}^k \cdot \underline{A}_{l+1}^k|_{\rho=r_l} \quad (9)$$

where $\underline{A}_l^k = [A_{1l}^k A_{2l}^k B_{1l}^k B_{2l}^k]^T$, and $\underline{\underline{X}}_l^k$ is given in the Appendix.

From that we easily proceed to the following equation:

$$\underline{A}_{l+1}^k = \underline{\underline{X}}_{\text{tr}_l}^k \cdot \underline{A}_l^k|_{\rho=r_l} \quad (10)$$

with

$$\underline{\underline{X}}_{\text{tr}_l}^k = (\underline{\underline{X}}_{l+1}^k)^{-1} \underline{\underline{X}}_l^k.$$

Now we see that the amplitudes in the layer $(l+1)$ can be expressed in terms of the amplitudes of lth layer. If we apply this algorithm consecutively to every pair of adjacent layers, starting from the innermost, we arrive at the following formula:

$$\underline{A}_L^k = \underline{\underline{\mathbf{X}}}_{\mathbf{Tr}}^{\mathbf{k}} \underline{A}_1 \quad (11)$$

where *the global transfer matrix* $\underline{\underline{\mathbf{X}}}_{\mathbf{Tr}}^{\mathbf{k}}$ is defined as

$$\underline{\underline{\mathbf{X}}}_{\mathbf{Tr}}^{\mathbf{k}} = \prod_{l=1}^{L-1} \underline{\underline{X}}_{\text{tr}_l}^k. \quad (12)$$

The transfer matrix approach to the analysis of IG has several advantages, namely

- the complexity of the inner structure of IG is hidden in $\underline{\underline{\mathbf{X}}}_{\mathbf{Tr}}^{\mathbf{k}}$. In subsequent steps of the analysis the IG structure is only referred to through the transfer matrix.
- the transfer matrix approach can be easily algorithmized

B. Fields in AG's

The AG's may have a variety of cross-sectional shapes, ranging from rectangular waveguides open at one side, sectoral guides, to parallel plate guides with magnetic or electric walls. We require however the Helmholtz equation formulated in AG region to be separable. Such a general formulation lets us handle a wide class of AG's.

The solution of Maxwell's equations is expressed as a series of type E and H modes, complete in an AG region

$$D_x^{\perp,i} = \sum_n e_n^i D_{xn}^{\perp,i}$$
$$\tilde{H}_x^{\perp,i} = \sum_n h_n^i H_{xn}^{\perp,i} \quad (13)$$

where i denotes ith AG, n—nth eigenfunction, and e_n^i, h_n^i are unknown amplitudes. Superscript $\perp$ indicates quantities defined in AG's.

In accordance with the earlier formulation, we assume the eigenfunctions $D_x^{\perp,i}$ and $H_x^{\perp,i}$ in the following form:

$$D_{xn}^{\perp,i\pm} = e^{-\jmath\beta x} \Phi_n^{i\pm}(q_1) \Upsilon_n^{i\pm}(q_2) \quad (14)$$
$$\tilde{H}_{xn}^{\perp,i\pm} = e^{-\jmath\beta x} \Psi_n^{i\pm}(q_1) \Omega_n^{i\pm}(q_2) \quad (15)$$

where: q_1, q_2 are transverse coordinates of a system in which AG is defined, (y and z in case of Fig. 1).

The transverse components can be found from [13]

$$\begin{bmatrix} E_{q1} & \tilde{H}_{q_1} \\ E_{q2} & \tilde{H}_{q_2} \end{bmatrix} = \frac{1}{\delta} \begin{bmatrix} -\frac{1}{h_2}\frac{\partial}{\partial q_2} & \frac{1}{h_1}\frac{\partial}{\partial q_1} \\ \frac{1}{h_1}\frac{\partial}{\partial q_1} & \frac{1}{h_2}\frac{\partial}{\partial q_2} \end{bmatrix} \times \begin{bmatrix} -jk_0/\epsilon_0 \tilde{H}_x & jk_0 D_x \\ -\frac{1}{\epsilon_0 \epsilon_d}\frac{\partial}{\partial x} D_x & -\frac{1}{\mu}\frac{\partial}{\partial x}\tilde{H}_x \end{bmatrix} \quad (16)$$

where h_1, h_2 are metric coefficients of coordinate system, and δ is a separation constant.

C. Field Matching

At this stage of the analysis we have the general solutions to Maxwell's equations in each distinguished region of the structure. To solve the boundary problem however, we have to *match the fields*, i.e., to ensure the continuity of the fields on all the interfaces between regions. Regions IG and AG's partially overlap (Fig. 1), and therefore a number of interfaces can be specified on which the continuity conditions for the fields can be imposed. Of practical importance are only these interfaces, on which it is possible to take advantage of the orthogonality properties of eigenfunctions i.e., interfaces ξ and ζ. Furthermore, a number of options are available: we can match all tangential components on ξ or on ζ, or we can formulate E field conditions on one and H fields on the other interface or vice versa. The latter options offer better numerical behavior of the resulting algorithm, since they lead to a bi-directional orthogonalization, which provides more flexibility in selecting the number of eigenfunctions taken for field approximation in the regions of the structure [8], [12]. We will use this approach henceforth.

Let us consider the continuity conditions for $\vec{E}$ fields on ζ, and for the $\vec{H}$ fields on ξ (for the sake of clarity we assume in this section that AG's are defined in rectangular coordinates, as in Fig. 1)

$$\left.\begin{aligned} \tilde{H}_x^\circ &= \textstyle\sum_{i=1}^M \tilde{H}_x^\perp \mathcal{B}_i(\varphi) \\ \tilde{H}_\varphi^\circ &= \textstyle\sum_{i=1}^M \tilde{H}^\perp \vec{a}_\varphi \mathcal{B}_i(\varphi) \end{aligned}\right|_\xi \tag{17}$$

$$\left.\begin{aligned} E_x^\circ &= \textstyle\sum_{i=1}^M E_x^\perp \mathcal{B}_i(\varphi) \\ \textstyle\sum_{i=1}^M \vec{E}^\circ \vec{a}_{z_i} \mathcal{B}_i(\varphi) &= \textstyle\sum_{i=1}^M E_{z_i}^\perp \mathcal{B}_i(\varphi) \end{aligned}\right|_\zeta \tag{18}$$

where $\mathcal{B}$ is a function selecting ith AG region.

To transform (18) into an algebraic system we take the inner products of its both sides with every function from the set of IG eigenfunctions, $\{e^{jk\varphi}\}$, with the definition of the inner product ensuring orthogonality

$$\langle f \mid g \rangle_\xi \stackrel{\text{def}}{=} \oint_\xi f g^\star \, d\xi = \int_0^{2\pi} f g^\star R_d \, d\varphi. \tag{19}$$

The operation can formally be written as follows:

$$\left\langle \begin{matrix} \tilde{H}_x^\circ \\ \tilde{H}_\varphi^\circ \end{matrix} \middle| \, e^{-jk\varphi} \right\rangle_\xi = \left\langle \begin{matrix} \sum_{i=1}^M \tilde{H}_x^\perp \mathcal{B}_i(\varphi) \\ \sum_{i=1}^M \tilde{H}_\varphi^\perp \mathcal{B}_i(\varphi) \end{matrix} \middle| \, e^{-jk\varphi} \right\rangle_\xi . \tag{20}$$

As a result we obtain a matrix formula

$$\underline{\underline{T}} \begin{bmatrix} \underline{A} \\ \underline{B} \end{bmatrix} = \underline{\underline{\Delta}} \begin{bmatrix} \underline{\mathbf{e}} \\ \underline{\mathbf{h}} \end{bmatrix} \tag{21}$$

where $\underline{\underline{T}}$ is built of diagonal sub matrices, $\underline{\underline{\triangle}}$ is dense and $[\underline{A}\,\underline{B}]^T$ and $[\underline{\mathbf{e}}\underline{h}]^T$ are vectors storing amplitudes of eigenfunctions of IG and AG's, respectively [12].

A similar procedure is applied to (18). In this case, we take the inner product of its both sides with every eigenfunction of AG's. The appropriate inner product for this operation is defined as follows:

$$\langle f \mid g^{\perp_i} \rangle_\zeta \stackrel{\text{def}}{=} \oint_\zeta f (g^{\perp_i})^\star \mathcal{B}_i(\varphi) \, d\zeta = \int_{-a_i}^{a_i} f (g^{\perp_i})^\star \, dz_i \tag{22}$$

and the formal description of the procedure is:

$$\langle E_x^\circ \mid \Upsilon_n^i(z_i) \rangle_\zeta = \langle E_x^\perp \mid \Upsilon_n^i(z_i) \rangle_\zeta \tag{23}$$

$$\left\langle \vec{E}^\circ \vec{a}_{z_i} \mid \Omega_n^i(z_i) \right\rangle_\zeta = \langle E_{y_i}^\perp \mid \Omega_n^i(z_i) \rangle_\zeta \tag{24}$$

$$\text{for } i = 1, 2 \cdots, M \text{ and } n = 0, \cdots, N_i. \tag{25}$$

This operation yields the following matrix relation

$$\underline{\underline{V}} \begin{bmatrix} \underline{A} \\ \underline{B} \end{bmatrix} = \underline{\underline{\Lambda}} \begin{bmatrix} \underline{\mathbf{e}} \\ \underline{\mathbf{h}} \end{bmatrix} \tag{26}$$

where $\underline{\underline{\Lambda}}$ is built of diagonal matrices and $\underline{\underline{V}}$ is dense [12].

In both (21) and (26) we notice the same vectors of unknown amplitudes. One of them can be eliminated which leads to a homogeneous system of algebraic equations. After setting its determinant to zero, the dispersion equation is obtained

$$\left[\underline{\underline{\Lambda}} - \underline{\underline{V}} (\underline{\underline{T}})^{-1} \underline{\underline{\triangle}} \right] \begin{bmatrix} \underline{\mathbf{e}} \\ \underline{\mathbf{h}} \end{bmatrix} = 0. \tag{27}$$

III. Application of FFT

Critical from the point of view of the computation efficiency is the evaluation of the inner products. The inner products encountered in our algorithm have the form

$$S_k = \int_{-\theta_1}^{\theta_1} \mathcal{S}(\varphi) e^{-jk\varphi} \, d\varphi$$

where S is a certain function of φ. These products must be computed for k ranging from 1 to K, where K is number of eigenfunctions taken into account in the IG. Simple transformation of variables, and a modification of S

$$\bar{\mathcal{S}}(\varphi) = \begin{cases} 0 & |\varphi| > \theta_1 \\ \mathcal{S} & |\varphi| \le \theta_1 \end{cases} \qquad \bar{\varphi} = \varphi + \pi$$

leads to the modified formula for S_k

$$S_k = 2\pi(-1)^k \frac{1}{2\pi} \int_0^{2\pi} \bar{\mathcal{S}}(\bar{\varphi}) e^{-jk\bar{\varphi}} d\bar{\varphi}.$$

In this formula we easily recognize a term which represents a Fourier expansion coefficient of function $\bar{\mathcal{S}}(\varphi)$ and which may be efficiently computed by FFT. Using this strategy we have gained three-fold increase in computational speed and two-fold reduction in computer storage.

IV. Verification and Results

Numerous numerical and experimental tests have been carried out in order to verify the method. Various hollow and homogeneously filled waveguides were evaluated using the program, and the results obtained matched the known analytical formulae. In further tests, parameters of various dielectric guides were computed for which solutions had previously been published. For example, in Table I results of our, and previously published computations of resonance

TABLE I
COMPUTED AND MEASURED RESONANCE FREQUENCIES (IN GHz) OF QUASI-TE_{101} AND QUASI-TE_{201} MODES OF AN "IMAGE" GUIDE OF FIG. 5

Mode	Present method	Measured [15]	Theory [15]	Theory [16]
TE_{101}	1.263	1.263	1.267	1.269
TE_{201}	1.678	1.672	1.700	1.678

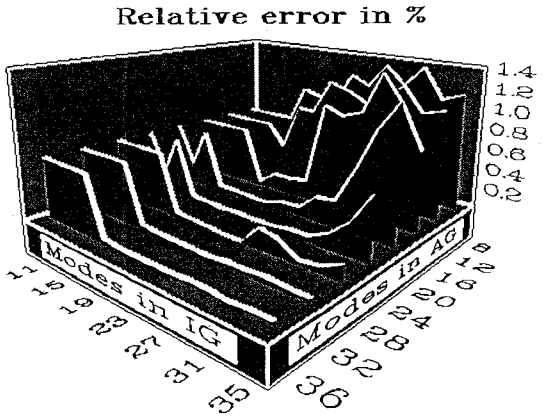

Fig. 4. Error in the cut-off frequency of the fundamental mode of a hollow rectangular waveguide as a function of numbers of modes taken in IG and AG's regions. Waveguide dimensions: 22.86 × 10.16 mm.

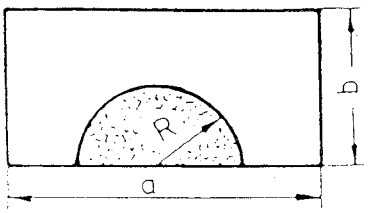

Fig. 5. Shielded "image" guide. $\epsilon = 2.495$, $R = 5$ cm, $a = 20$ cm, $b = 10$ cm. Length of the resonator: 11.1 cm.

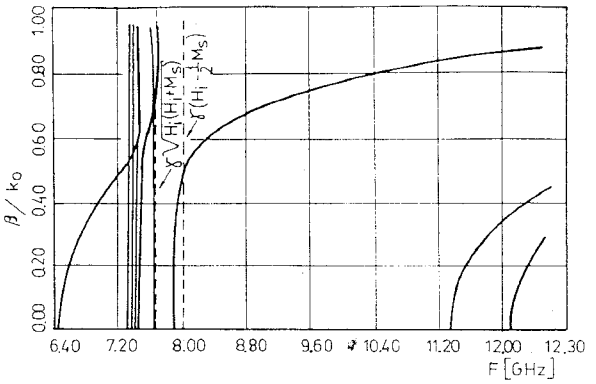

Fig. 6. Dispersion characteristics of a rectangular waveguide comprising longitudinally magnetized ferrite rod. $M_s = 1750\frac{1}{4\pi}\frac{kA}{m}$, $H_i = 1.143 * M_S$. Waveguide dimensions 22.86 × 10.16 mm.

frequencies of an "image" line are presented—a high accuracy of our method can be observed.

A standard, hollow rectangular waveguide was used to test the convergence properties of the method. This simple structure is not a trivial one from the standpoint of the complexity of the method used in computations of its parameters. Since the computations of cutoff frequencies are often particularly prone to errors, we used them as a target in testing. The results, presented in Fig. 4, display typical features of field (or mode) matching method, namely:

- the method can provide very accurate results, the error is less then 0.03% if 20–30 eigenfunctions are taken in IG and AG's,
- if the number of eigenfunctions taken into account in IG substantially differs from that of AG's, a relative convergence effect may be observed [14], and
- as the number of modes increases the area of low relative error widens.

In particular, it can be observed in Fig. 4, that if the number of modes in IG is low, the method may converge to a solution which carries a relative error of 1%. On the other hand, if the number of modes in IG equals to the total number of modes in AG's, a high accuracy is obtained, even if low number of modes is taken into account.

Dispersion characteristics of a rectangular waveguide containing a magnetized ferrite rod are presented in Fig. 6. As the frequency approaches $f_1 = \gamma\mu_0\sqrt{H_i(H_i + M_s)}$ (where gyromagnetic ratio $\gamma = 27.997 \cdot 10^9$ [C/kg]), volume magnetostatic waves appear and the fundamental (dynamic) mode transforms into a magnetostatic one. For frequencies ranging from f_1 to $f_2 = \gamma\mu_0(H_i + 0.5M_s)$ surface magnetostatic waves may be excited, some having backward wave nature. Near f_2 the second cutoff frequency of the fundamental mode can be observed. The remaining part of the characteristics is similar to those of a dielectric loaded waveguide [12].

The proper behavior of the method in computations of ferrite loaded structures was verified experimentally. A section of a rectangular waveguide loaded with a longitudinally magnetized ferrite rod was terminated with metallic walls to form a resonator. The resonance frequency was computed and measured experimentally as a function of the applied external biasing magnetic field as shown in Figs. 7 and 8. The theoretical and experimental data are in good agreement which validates the method. An interaction between ferrite medium and e.m. wave weakens when the ferrite rod is shifted from the center toward the narrow waveguide wall as illustrated in Fig. 7. Conversely, if the ferrite material is positioned close to the wide waveguide wall the interaction with e.m. field intensifies and, moreover, the sensitivity to the strength of the biasing magnetic field increases—Fig. 8. Although this type of structure is widely used (e.g., in phase shifters) it has not been rigorously analyzed before.

In a cross-rectangular waveguide comprising longitudinally magnetized ferrite rod, a Faraday rotation phenomenon can be observed. This structure provides substantial flexibility in shaping of the frequency characteristics as shown in Fig. 9, and is potentially useful in ferrite devices.

V. CONCLUSION

We have presented a method of analysis of waveguides of complex cross-sectional geometry, comprising longitudinally magnetized ferrite-dielectric rods. The method can be used to analyze a wide class of waveguides, including rectangular

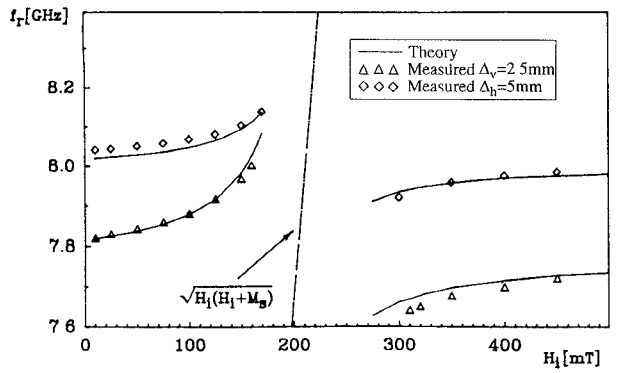

Fig. 7. Resonance frequency versus external dc magnetic field in resonator consisting of a section of rectangular guide loaded with a ferrite rod. (ϕ = 3 mm, $M_s = 950\frac{1}{4\pi}\frac{kA}{m}$, $\epsilon_f = 13$), $a = 22.86$ mm, $b = 10.16$ mm. Δ_h—offset of the rod from the center toward narrow waveguide wall.

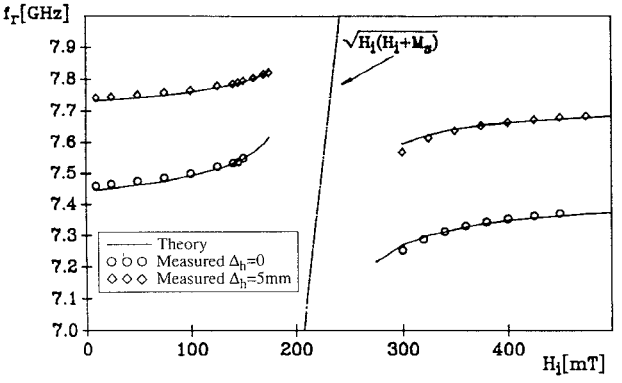

Fig. 8. Resonance frequency versus external dc magnetic field in resonator consisting of a section of rectangular guide loaded with a ferrite rod. (ϕ = 3 mm, $M_s = 1750\frac{1}{4\pi}\frac{kA}{m}$, $\epsilon_f = 13.5$), $a = 22.86$ mm, $b = 10.16$ mm. Δ_h, Δ_v—offset of the rod from the center toward narrow or wide waveguide wall, respectively.

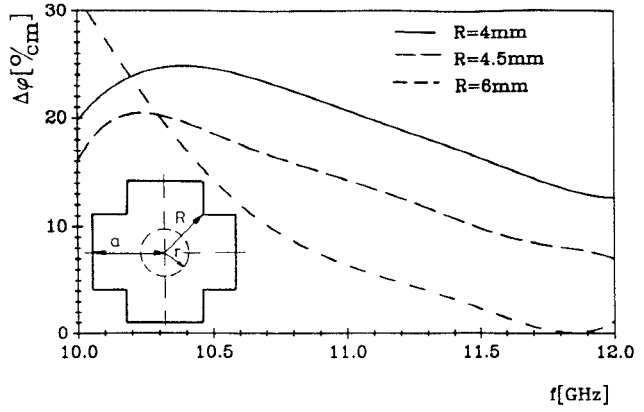

Fig. 9. Rotation of the polarization plane in a cross-rectangular waveguide comprising longitudinally magnetized ferrite. $r = 2.5$ mm, $a = 7$ mm, $M_s = 2200\ \frac{1}{4\pi}\frac{kA}{m}$, $H_i = 0$, $\epsilon_f = 13.5$.

waveguides loaded with ferrite rods. These structures have not been rigorously analyzed before. In computations of inner products encountered in the method we used FFT techniques which resulted in greater computational speed and reduced computer storage requirements. The numerical and experimental results provided validate the method of analysis presented in the paper.

APPENDIX

$$\underline{\underline{X}}_l = \begin{bmatrix} u_2^l J_{l1}' + u_1^l J_{l1} & u_2^l Y_{l1}' + u_1^l Y_{l1} & v_2^l J_{l2}' + v_1^l J_{l2} & v_2^l Y_{l2}' + v_1^l Y_{l2} \\ u_3^l J_{l1} - u_4^l J_{l1}' & u_3^l Y_{l1} - u_4^l Y_{l1}' & v_3^l J_{l2} - v_4^l J_{l2}' & v_3^l Y_{l2} - v_4^l Y_{l2}' \\ \frac{1}{\epsilon_0 \epsilon_{fl}} J_{l1} & \frac{1}{\epsilon_0 \epsilon_{fl}} Y_{l1} & \frac{1}{\epsilon_0 \epsilon_{fl}} R J_{l2} & \frac{1}{\epsilon_0 \epsilon_{fl}} R Y_{l2} \\ S J_{l1} & S Y_{l1} & J_{l2} & Y_{l2} \end{bmatrix}$$

where

$$u_1^l = \frac{1}{\epsilon_0 \epsilon_{fl}} \frac{k}{\rho} \frac{\beta}{\chi_1^2} \qquad v_1^l = \frac{1}{\epsilon_0 \epsilon_{fl}} \frac{k}{\rho} \frac{\beta}{\chi_2^2} R$$

$$u_2^l = j \frac{k_0}{\epsilon_0 \chi_1^2} S \qquad v_2^l = j \frac{k_0}{\epsilon_0 \chi_2^2}$$

$$u_3^l = \frac{1}{\chi_1^2} \frac{k}{\rho} \left(j k_0 \frac{\mu_{al}}{\mu_l} + \frac{\beta}{\mu_l} S \right) \qquad v_3^l = \frac{1}{\chi_2^2} \frac{k}{\rho} \left(j k_0 \frac{\mu_{al}}{\mu_l} R + \frac{\beta}{\mu_l} \right)$$

$$u_4^l = j \frac{k_0}{\chi_1^2} \qquad v_4^l = j \frac{k_0}{\chi_2^2}$$

and $J_{l1,2}$ (or Y) denote appropriate Bessel function of argument $\chi_{1,2}^l \rho$, while prime denotes differentiation with respect to ρ.

REFERENCES

[1] S. M. Saad, "Review of numerical methods for the analysis of arbitrarily shaped microwave and optical dielectric waveguides," *IEEE Trans. Microwave Theory Tech.*, vol. MTT-33, pp. 894–899, Oct. 1985.

[2] T. Itoh, Ed., *Numerical Techniques for Microwave and Millimeter-Wave Passive Structure*. New York: Wiley, 1989.

[3] N. Kukutsu, N. Yoshida, and I. Fukai, "Transient analysis of ferrite in three-dimensional space," *IEEE Trans. Microwave Theory Tech.*, vol. MTT-36, pp. 114–125, Jan. 1988.

[4] M. Okoniewski and J. Mazur, "An accurate, field matching analysis of waveguide of complex cross-sectional geometry loaded with magnetized ferrite rods," in *IEEE Microwave Theory Tech. Soc. Int. Symp. Dig.*, Boston, MA, 1991, pp. 181–184.

[5] ——, "Multimode *S*-matrix for ferrite planar multiport circuits," in *Proc. 8th Colloquium on Microwave Commun.*, Budapest, Hungary, 1986.

[6] J. Lauterjung, "Abstrahlungs—und beugungsprobleme in hohleiterstrukturen mit isotropen und magnetish gyrotropen kreiszylindrischen streukörpern," Dissertation, Technishen Hochscule Darmstad, 1982.

[7] R. Gesche and N. Löchel, "Scattering by a lossy dielectriccylinder in a rectangular waveguide," *IEEE Trans. Microwave Theory Tech.*, vol. MTT-36, pp. 137–144, 1988.

[8] M. Okoniewski and J. Mazur, "Waveguides with complex cross-sectional geometry containing longitudinal dielectric rods," in *Proc. URSI Int. Symp.*, Stockholm, Sweden, 1989, pp. 114–116.

[9] F. E. Gardiol, "Propagation in rectangular waveguide loaded with slabs of anisotropic materials," Ph. D. dissertation, Louvain, 1969.

[10] A. G. Gurevich, *Ferrites at Microwave Frequencies*. Heywood, 1960.

[11] B. Lax and K. J. Button, *Microwave Ferrites and Ferrimagnetics*. New York: McGraw-Hill, 1962.

[12] M. Okoniewski, "Branched wave-guiding structures, their theory and analytical applications," Ph.D. dissertation, Technical University of Gdańsk, 1990 (in Polish).

[13] M. Mrozowski and J. Mazur, "Analysis of a circularly cylindrical resonator filed with axially magnetized strata of gyromagnetic media," *J. Electromagn. Waves Appl.*, vol. 3, no. 3, pp. 269–276, Mar. 1989.

[14] R. Mittra and W. Lee, *Analytical Techniques in Theory of Guided Waves*. New York: Macmillan, 1971.

[15] W. Beier, "Waves and evanescent fields in rectangular waveguide filled with a transversely inhomogeneous dielectric," *IEEE Trans. Microwave Theory Tech.*, vol. MTT-18, pp. 696–705, Oct. 1970.

[16] M. Mrozowski, "IEEM-FFT A Fast and efficient tool for rigorous computations of propagation constant and field distribution in dielectric guides with arbitrary cross-section and permittivity profile," *IEEE Trans. Microwave Theory Tech.*, vol. 39, Feb. 1991.

Michał Okoniewski (M'87) received the M.Sc. and Ph.D. (with honors) degrees in electrical engineering from the Technical University of Gdańsk, Poland in 1984 and 1991, respectively.

From 1984 to 1986 he was with The Fluid Flow Machinery Institute, the subsidiary of Polish Academy of Sciences. In 1986 he joined the faculty at the Technical University of Gdańsk, where he taught courses and carried out research in the field of the theory and applications of electromagnetic fields. In 1992 he was awarded the Canadian NSERC International Postdoctoral Fellowship and joined the University of Victoria, Victoria, British Columbia, Canada, where he is now a research associate. He is interested in electromagnetic wave interactions with complex media (including biological and gyrotropic materials), numerical methods in electromagnetics, microwave hyperthermia, and passive devices.

Jerzy Mazur graduated from the Technical University of Gdańsk, Poland in 1969, and received the Ph.D. and D.Sc. degrees in electrical communication engineering from the same university in 1976 and 1983, respectively.

He is currently a full professor in the Faculty of Electronics, Technical University of Gdańsk. His research interests are concentrated on electromagnetic field theory and integrated circuits for microwave and millimeter wave applications.

Dr. Mazur is a member of the Electromagnetic Academy.